Tellus (1988), *40A*, 303–323

Numerical simulation of flows with locally characteristic boundaries

By ROBERT N. MILLER*, *Lamont-Doherty Geological Observatory, Palisades, NY 10964, USA* and ANDREW F. BENNETT*, *Institute of Ocean Sciences, Sidney, BC V8L-4B2, Canada*

(Manuscript received 4 April 1987; in final form 5 October 1987)

ABSTRACT

Numerical modeling of oceanic circulation on synoptic scales leads to interesting boundary value problems. Data sets with sufficient spatial resolution to be useful for model initialization are usually restricted to limited areas. Consequently, open boundary models are required, but they do not appear to yield well-posed problems, and it is not clear how the schemes currently in use in ocean forecasting experiments perform under such circumstances. The difficulties which occur due to incompatibilities in the specification of boundary conditions may arise in cases in which the open region is embedded in a larger domain in which the flow is very smooth. These effects are thus distinct from the development of discontinuities which form as a result of advection of nonuniform fields, i.e., kinematic frontogenesis. The practical effect of the results presented here is to emphasize the need for regular reinitialization of the forecast fields through some data assimilation process.

The difficulties with the boundary value problem are illustrated here through simple analytical examples, and through nonlinear numerical experiments using finite difference and finite element methods. The utility of numerical filters is examined. A review of relevant theoretical investigations is also presented.

1. Introduction

Regional models with open boundary conditions are finding increasing use in the study of oceanic synoptic variability. One example of such a model is the Harvard Open Ocean Model (see Miller et al. (1983) for details) which has been used in a number of studies with real and simulated data (Miller and Robinson, 1984; Robinson and Leslie, 1985; Robinson et al., 1984). The model uses quasigeostrophic physics and the open boundary conditions proposed by Charney et al. (1950; hereafter CFvN), that is, at each depth, the normal velocity is specified everywhere on the boundary but the potential vorticity is specified only where the normal velocity is directed inward. We report here on a series of analytical and numerical calculations which illustrate the properties of this fundamentally nonlinear boundary value problem.

To motivate their choice of boundary condition, Charney et al. (1950) considered two-dimensional flow on the surface of a circular cylinder. Being of finite length, the cylinder had two rims. Uniform inflow was imposed on one rim and uniform outflow on the other. Well behaved solutions were explicitly constructed. It may be remarked that the flow domain (the finite section of the cylinder) was multiply connected. Technically speaking, this means that there are closed curves in the domain which cannot be shrunk to points without leaving the domain: consider any loop around the cylinder. Intuitively, if a right circular cylinder were projected onto a plane normal to its axis (literally, by shining a light down the cylinder and onto a screen), then the resulting annulus would have a boundary comprised of two circles, one inside of

* Present affiliation: College of Oceanography, Oregon State University, Corvallis, Oregon, 97331 USA.

the other. Under this projection, a loop around the cylinder would map into a closed curve surrounding the central hole in the annulus. Judovich (1964) investigated incompressible flow in such multiply connected planar domains with the CFvN boundary condition. He proved the existence and uniqueness of smooth solutions provided that the data on the boundary are smooth and that the normal velocity on each part of the boundary is bounded away from zero. In the present context of incompressible flows, the divergence theorem implies that this latter requirement can only be met on the boundary of a multiply connected domain. The net inflow across the single boundary of a simply connected domain must be zero, so the normal velocity must change sign somewhere on such a boundary. Clearly, the illustrative example of Charney et al. was judiciously chosen. It should be remarked that in 1949 Kochin considered three dimensional flow through a finite section of a solid cylinder, obtaining results similar to those of Judovich (1964). Kochin's work was actually completed by Dalidze, and this Russian work has been translated into English; see our reference to Kochin (1980), where the original Russian references may also be found.

It is implied above that there are difficulties with points on the boundary where the imposed normal velocity changes sign, that is the flow is locally tangential. The reason is that the fluid particle paths are the characteristics of the advection equation for vorticity. The latter is in fact quasilinear since the advecting velocities are determined, albeit nonlocally, by the vorticity field itself, as well as by the boundary data. Since data can only be continued or extended in characteristic directions, it follows that the interior solution is not well determined, at least near the boundary where the flow is tangential at some instant, and possibly elsewhere at later times as a consequence of the tendency of the physical system to propagate singularities along characteristics (see, e.g., Whitham, 1974).

Some more recent studies of the CFvN boundary conditions would appear to be at odds with the above remarks, in that proofs of well-posedness in simply connected domains are offered. However these proofs assume either extraordinarily special data (Sensenig, 1959) or else establish uniqueness and continuous dependence of the solution upon data but do not prove existence of smooth solutions (Sundström, 1969; Fix, 1975).

The practical significance of the ill-posed nature of the initial-boundary value problem is that computed vorticity gradients grow in time without bound and these values also diverge as resolution is increased. This differs from the well known process of kinematic frontogenesis, in which nonuniform advection in planar fluid motion can also result in unbounded gradients. However, such a genuine physical process is not dependent upon numerical resolution and special numerical techniques are required.

An expanded description of the theoretical results mentioned above is given in Section 2. In Section 3, we present analytical examples which illustrate the difficulties due to "characteristic points" on the boundary. The theory and analytical examples are complemented by computations in Section 4. Implications for ocean modeling are discussed in the summary Section 5.

2. A survey of theoretical results

As noted above, Sundström (1969) proposed a proof that the inviscid quasigeostrophic potential vorticity equations with CFvN boundary conditions constituted a well posed problem, but Bennett and Kloeden (1978) pointed out that Sundström's proof depends on a bound for the normal derivative of the vorticity on the boundary and that such a bound, in general, does not exist. Fix (1975) presented a proof of convergence of the finite element method for this problem which suffered from the same defect (see his discussion on pp. 378–379). We shall present explicit examples in Section 3 of linearized problems in which the normal derivative of vorticity near the boundary is unbounded.

Bardos et al. (1979) considered the problem of convergence of solutions of quasilinear parabolic problems as the diffusivity vanishes. In Bardos et al. (1979), the boundary value problem for the equation

$$\frac{\partial \zeta_\varepsilon}{\partial t} + \operatorname{div}[f(\zeta_\varepsilon, x, t)] + g(\zeta_\varepsilon, x, t) = \varepsilon \nabla^2 \zeta_\varepsilon$$

was examined. This is a parabolic equation, and the solution must be specified on the entire boundary. The behavior of the ζ_ε as $\varepsilon \to 0$ was invstigated and it was proved that for any sequence $\varepsilon_m \to 0$ there is a subsequence of the ζ_ε which converges in the L^1 sense. This limiting function, however, will not in general have a bounded derivative. The boundary conditions satisfied by the limiting functions for vanishing viscosity were shown to be the CFvN conditions in special cases.

Majda and Osher (1975) studied the general linear hyperbolic problem:

$$L\zeta = \zeta_t - \sum_{j=1}^{m} A_j(t,x)\frac{\partial \zeta}{\partial x_j} - C(t,x)\zeta = F,$$

where ζ is a k vector and the A_j and C are $k \times k$ matrices, in cases where the boundary is uniformly characteristic. In this setting, "uniformly characteristic" means that if n is the outer normal to the boundary, with components $(n_1, n_2 \ldots n_m)$, then, for all x and t on the boundary, there is a constant k_1 with:

$$\text{rank}\left\{\sum_{j=1}^{m} A_j(t,x)n_j\right\} = k_1 < k. \tag{1}$$

For this problem and suitable boundary conditions, existence and uniqueness of solutions is proved. It is the defective rank of the matrix in (1) that makes the boundary characteristic; the assumption of constant rank is necessary for their techniques to work, and that assumption does not hold in the CFvN case. In fact, Majda and Osher note specifically that "This assumption ... is too restrictive to handle all boundaries and linearizations for the shallow water equations ... for these equations the ranks can change over thin subsets of ... (the boundary)". This is precisely the geometrical case of interest here, but for the quasigeostrophic rather than the shallow water system.

The specific problem of well posed boundary conditions for the quasigeostrophic system in a simply connected domain was investigated by Sensenig (1959); see also a brief description in Forsythe and Wasow (1960). Since Sensenig's work is not widely available, his major results will be stated in some detail.

The quasigeostrophic system on the f-plane may be written:

$$\frac{\partial \zeta}{\partial t} + J(\psi,\zeta) = 0 \tag{2a}$$

$$\nabla^2\psi - \lambda^2\psi = \zeta \tag{2b}$$

where ψ and ζ are functions of x, y, and t, λ is a positive constant and

$$J(\psi, \bullet) = (\psi_x \partial/\partial y - \psi_y \partial/\partial x).$$

We consider the problem in the half plane $y > 0$ for $0 < t < c$, where c = some positive constant. We prescribe initial conditions for both ψ and ζ, ψ on the entire x-axis at all times, and ζ at inflow points on the x-axis, i.e., those points at which $\psi_x > 0$. If ψ and ζ constitute a solution to (2b) then:

$$\psi = \frac{1}{2\pi}\int_0^{\infty}\int_{-\infty}^{\infty} g(x,y,\xi,\eta)\zeta(\xi,\eta,t)\,d\xi\,d\eta - \frac{\lambda y}{\pi}\int_{-\infty}^{\infty}\psi(\xi,0,t)K'(\lambda v)v^{-1}\,d\xi, \tag{3}$$

where

$$v = [(\xi - x)^2 + y^2]^{1/2}$$

$$g(x,y,\xi,\eta) = K(\lambda\bar{\rho}) - K(\lambda\rho)$$

$$\rho = [(\xi - x)^2 + (\eta - y)^2]^{1/2}$$

$$\bar{\rho} = [(\xi - x)^2 + (\eta + y)^2]^{1/2},$$

and K is the modified Bessel function of the second kind of order zero. Sensenig worked with the case in which ψ remains close to a linear function in x. Specifically, there are assumed to be constants a and b, with $a > 0$, such that $\psi_x - a$, $\psi - ax - b$ and ψ_y are bounded. A consistent restriction is placed on ζ, namely, $\zeta + \lambda^2(ax + b)$ is bounded. This latter form follows from (2b).

He then used these integrals to define weak solutions. Let Ψ be a smooth function on the domain in question, and let $(x(t), y(t))$ be the particle paths defined by considering Ψ as a streamfunction, i.e., solutions to:

$$\frac{dx}{dt} = -\Psi_y, \quad \frac{dy}{dt} = \Psi_x.$$

Let H be a function which is constant along particle paths and for which

$$\iint g(x,y;\xi,\eta)H(\xi,\eta,t)\,d\xi\,d\eta$$

exists. H is then called a Pseudo-Helmholtzian of Ψ. If H and Ψ satisfy (3) when substituted for ζ and ψ respectively, then they constitute a weak solution of (2). Next, let the outflow region of the boundary be bounded by the curves C_1 and C_2 in

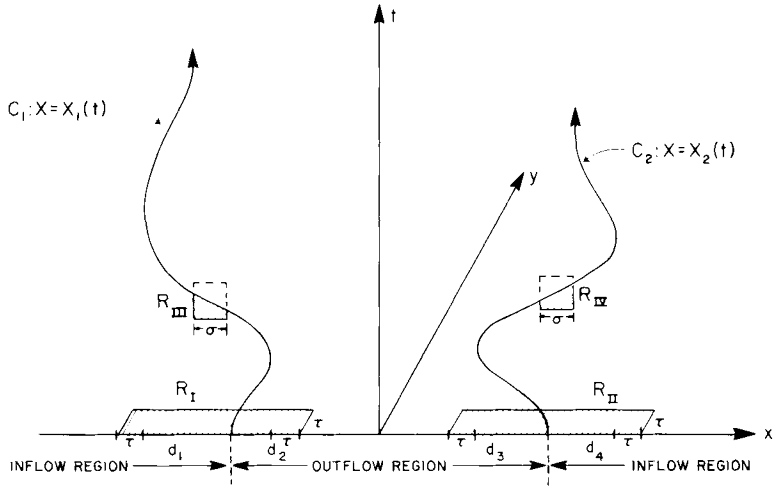

Fig. 1. Schematic diagram of boundary geometry in Sensenig's formulation of the problem. Hatched regions illustrate areas where the vorticity is prescribed to be constant. Curves C_1 and C_2 in the x–t plane form the boundaries of the outflow region of the boundary. d_1 and d_2 are the minimum and maximum respectively of the function $x_1(t)$; d_3 and d_4 are the minimum and maximum of $x_2(t)$. In regions $R_{\rm I}$ ($R_{\rm II}$) in the x–y plane, the initial vorticity is required to be p_1 (p_2), where p_1 and p_2 are constants. $R_{\rm III}$ is composed of a square of side σ centered at a point $(x_1(t_0), t_0)$, intersected with the inflow region. σ is a constant $< \tau$. The vorticity on $R_{\rm III}$ is required to be p_1. $R_{\rm IV}$ is similar, with the vorticity required to be p_2.

the x–t plane satisfying $x = x_1(t)$ and $x = x_2(t)$, where x_1 and x_2 are bounded and satisfy a uniform Lipschitz condition. Given sufficiently smooth initial and boundary conditions, Sensenig proved the existence of weak solutions Ψ of (2) with Ψ twice continuously differentiable at most points, i.e., (2b) is satisfied identically. Points which lie on particle paths which enter the region on C_1 or C_2 were specifically excluded; this can happen in the degenerate case in which the first and second tangential derivatives of the prescribed streamfunction on the boundary vanish. In order to obtain a true solution to (2) throughout the domain, Sensenig assumed the vorticity boundary conditions to be constant in space and time in neighborhoods of C_1 and C_2. He required further that the initial vorticity be constant in two strips in the x–y plane. These strips properly include the ranges of x_1 and x_2, and extend some finite distance into the domain in the y direction. These initial and boundary conditions are illustrated schematically in Fig. 1. The time domain of these smooth solutions was further restricted so that characteristics originating at distant points on the boundary or on the initial plane can not carry incompatible information to the vicinity of characteristic points. The consequence of such an occurrence is illustrated in the next section by simple linear analytical examples. These are rather stringent conditions. One might conceivably expect to flatten out the vorticity field, i.e., to impose a zero spatial derivative upon the initial and boundary conditions in a vicinity of the tangent curves x_1 and x_2, but requiring further that the vorticity remain constant in time is too restrictive in most practical cases.

The minimum necessary (though not necessarily sufficient) compatibility condition may be derived simply. Consider again the case of a flow occupying the half plane $y > 0$. At some point x on the boundary where the given normal velocity $v(x, 0, t) = \psi_x$ vanishes, the vorticity equation becomes:

$$\zeta_t(x, 0, t) + u(x, 0, t)\,\zeta_x(x, 0, t) = 0. \tag{4}$$

Now $\zeta_t(x, 0, t)$ and $\zeta_x(x, 0, t)$ are both given as part of the initial and boundary conditions, assuming the given functions are sufficiently smooth. Thus the vorticity equation and the boundary data impose a condition on the tangential velocity u which can not, in general, be met. The usual result is a discontinuity in ζ, emanating from the characteristic point along particle paths. Alternatively, we may rearrange the vorticity equation into the form:

$$\zeta_y(x,0,t) = -\frac{\zeta_t(x,0,t) + u(x,0,t)\,\zeta_x(x,0,t)}{v(x,0,t)}. \quad (5)$$

Clearly, if (4) is not satisfied, then, by virtue of (5), $\zeta_y \to \infty$ as the normal velocity $v \to 0$.

The theoretical picture, then, is not entirely clear. Earlier formulations presented as proofs involved invalid assumptions or overly restrictive compatibility conditions. Proper boundary conditions for boundary value problems with uniformly characteristic boundaries for hyperbolic equations have been established but the techniques do not apply because the boundary is not uniformly characteristic. This aspect of the problem is complicated by the fact that the quasigeostrophic potential vorticity equations have only one family of characteristics and thus do not constitute a strictly hyperbolic system. Still other work along classical lines (Bardos et al., 1979) suggests that the small viscosity limit of the quasigeostrophic potential vorticity equations with viscosity may not be smooth.

3. Examples of solutions of boundary value problems with unbounded derivatives

We now present examples of boundary value problems with CFvN type boundary conditions in which the normal derivatives at the boundary are unbounded. Sensenig's work implies that cases with time-varying boundary conditions are the most likely candidates for examples in which smooth initial and boundary conditions give rise to unbounded derivatives, since the case of constant boundary vorticity on inflow can be made to satisfy the hypotheses of his strongest existence theorem by forcing the boundary vorticity to be locally constant in neighborhoods of the characteristic points. For any given set of boundary conditions for this problem, one could envision a sequence of approximating functions, each of which would be constant in successively smaller neighborhoods of the characteristic points. The limiting behavior of the smooth solutions so obtained would be interesting, but we will not pursue that line of inquiry here. The relative tractability of the case of steady boundary conditions in steady flow is also suggested by a classical result attributed to Hadamard (J.-Y. Sun, personal communication). Given the equation:

$$(\nabla^2 \psi)_x = 0$$

on the unit disk, the specification of ψ on the unit circle and $\nabla^2 \psi$ on the left or right semicircle yields a well posed problem. The proof is elementary: by extending the boundary value of $\nabla^2 \psi$ into the interior of the disk along horizontal lines, the problem is reduced to the Dirichlet problem for Poisson's equation. We therefore choose unsteady problems for our examples.

For our first example, we consider the equation:

$$\zeta_t + U\zeta_x = 0 \quad (6)$$

where U is a positive constant on the domain consisting of all (x,y) in the unit disk and $t \in [0,\infty)$. The analog of the CFvN boundary conditions is to prescribe ζ initially and impose ζ on the left hand semicircle for all time. The value of ζ at any given point in this domain can be identified with a boundary or an initial value, so for any fixed point (x,y,t) in the solution region, $\zeta(x,y,t)$ depends continuously on the data. We will show, however, that ζ can have an unbounded derivative in any neighborhood of the characteristic points $(0,1)$ and $(0,-1)$. If we parameterize the boundary by the angle θ measured from the x axis, the inflow set is given by $\pi/2 < \theta < 3\pi/2$. If we prescribe the boundary condition $\zeta = e^{i(k\cos\theta + \omega t)}$, the interior solution will eventually become:

$$\zeta = \exp\{i[-\omega x/U + \omega t - (k + \omega/U)(1-y^2)^{1/2}]\},$$

which is not differentiable at $y = \pm 1$, the points at which the flow is tangent to the model region, unless $k + \omega/U = 0$. This is exactly the condition for a function of the form $\exp[i(kx + \omega t)]$ to be a solution of (6), or, alternatively, to satisfy the compatibility condition (5). Thus we see explicitly that even though ζ at any given point depends continuously on the data, its y derivative does not. This is an extremely weak singularity, and it is reasonable to ask about the behaviour of practical numerical schemes. In the spirit of the problem at hand, the boundary and initial conditions would be expected to come from some exterior flow consistent with the model, i.e., for the correct value of U, the boundary and initial conditions actually would satisfy $k + \omega/U = 0$. The major manifestation of truncation error in schemes for problems of this type is phase error, i.e., an nth order scheme would have simple harmonic solutions with $k + \omega/U = O(h^n)$, where h is the gridspacing. Therefore, for $y = 1 - h$, $(1 - y^2)^{1/2} = O(h^{1/2})$, and thus as h approaches zero, the $(k + \omega/U)/(1 - y^2)^{1/2}$ term in the derivative would be $O(h^{n-1/2})$. A reasonably accurate scheme would therefore converge smoothly to the consistent solution. However, in realistic ocean models, the phase error may not be controlled by the horizontal grid spacing h. In a baroclinic model with sparse vertical resolution, significant phase error can result from vertical truncation error. In the case of application of open ocean models to real data, uncertainty in the internal deformation radii can result in systematic errors in the phase speed of disturbances. In these cases it is plausible that the normal derivative of the computed solutions near the boundary in the vicinity of a tangent point might diverge as h approaches zero. In a nonlinear problem, it is also plausible that large vorticity gradients could be swept downstream and possibly be advected into the interior where instabilities may result.

A similar example may also be found with the horizontal strip enclosed by the lines $y = 0$ and $y = 2$ as its domain. Consider the equation:

$$\zeta_t + \zeta_x + \cos x\, \zeta_y = 0, \tag{7}$$

where ζ is to be prescribed on inflow, i.e., those points at which $\cos x$ is positive on $y = 0$ and those points at which $\cos x$ is negative on $y = 2$.

We define the streamfunction $\psi = -y + \sin x$, and write:

$$u = -\psi_y, \quad v = \psi_x.$$

The equation (7) is the statement that ζ is constant along particle paths. In this case of steady flow, i.e., steady ψ, the particle paths coincide with the streamlines. The point (x_0, y_0) in the domain lies on the streamline $\psi = \psi_0 = -y_0 + \sin x_0 = -y + \sin x$. To find the value of the solution ζ at (x_0, y_0) we find a point $\bar{x}$ where this streamline intersects the lower (or upper) boundary. Let us assume that this streamline enters the domain through the lower boundary at $x = \bar{x}$. We write:

$$\sin \bar{x} = -y_0 + \sin x_0. \tag{8}$$

Now let the boundary condition be given by:

$$\zeta(x, 0, t) = \zeta(x, 2, t) = B(x, t)$$

for x in the inflow set. We have:

$$\zeta(x_0, y_0, t_0) = B(\bar{x}, t_0 - [x_0 - \bar{x}]),$$

where $\bar{x}$ is a function of x_0 and y_0. We make use of (8) to calculate the derivatives of ζ at (x_0, y_0). Differentiating (8) yields:

$$\cos x_0 - \cos \bar{x}\, \partial \bar{x}/\partial x_0 = 0,$$

$$-1 - \cos \bar{x}\, \partial \bar{x}/\partial y_0 = 0;$$

so

$$\partial \zeta/\partial x_0 = \partial B/\partial x \frac{\cos x_0}{\cos \bar{x}} + \left[-1 + \frac{\cos x_0}{\cos \bar{x}} \right] \partial B/\partial t,$$

$$\partial \zeta/\partial y_0 = \left[\frac{-1}{\cos \bar{x}} \right] \partial B/\partial x + \left[\frac{-1}{\cos \bar{x}} \right] \partial B/\partial t,$$

where partial derivatives in the preceding two equations are evaluated at $x = \bar{x}$ and $t = t_0 - (x_0 - \bar{x})$. We now see explicitly the source of problems when $\bar{x}$ approaches $\pm\pi/2$ if

$$\partial B/\partial x|_{x=\bar{x}} + \partial B/\partial t|_{t=t_0-(x_0-\bar{x})} \neq 0.$$

We also see the source of Sensenig's hypothesis of steady flow in a neighborhood of the tangent set, i.e., boundary separating the inflow set from the outflow set, which he needs to prove smoothness of the weak solution. In our example, solutions will be smooth if we impose the weaker condition:

$$\partial B/\partial t + \partial B/\partial x = 0$$

on the tangent set; this condition is exactly equation (4) for this problem.

Consider now the region of the x axis near $x = -\pi/2$, and let $B(x, t) = \sin(kx + \omega t)$. Examine the solution at the point $x_0 = -\pi/2$, $y_0 = \varepsilon/2$, where $\varepsilon \ll 1$. This point lies on a characteristic which intersects the horizontal line $y = 2$, which forms the top of the domain. Let $(\bar{x}, 2)$ be the point at which this characteristic intersects the upper boundary. We then have $-2 + \sin \bar{x} = -1 - \varepsilon/2$, so $\sin \bar{x} = 1 - \varepsilon/2$. We note from Fig. 2 that $\bar{x}$ lies just to the right of $x = -3\pi/2$; therefore let $\bar{x} = -3\pi/2 + h$. Then $\sin(-3\pi/2 + h) = \cos h = 1 - h^2/2 + O(h^4)$, so $h = \varepsilon^{1/2} + O(\varepsilon)$.

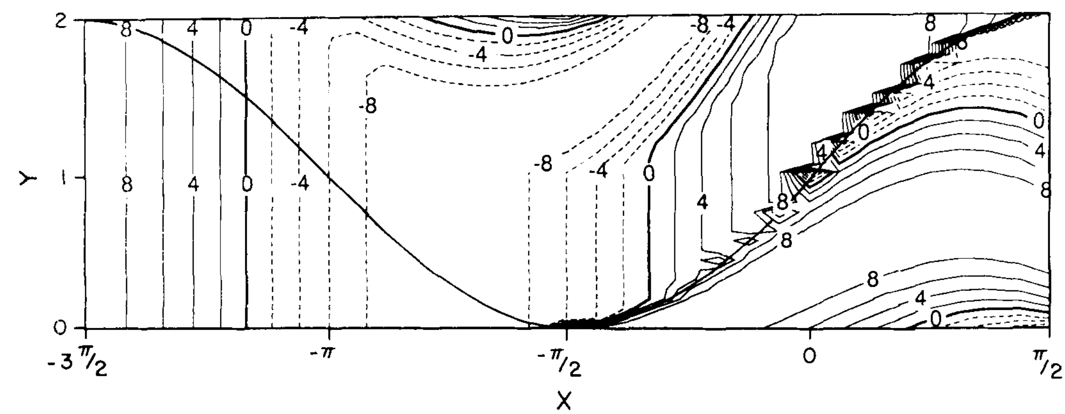

Fig. 2. Map of analytic solution to eq. (7) with $\psi = -1$ streamline drawn in. Note small scale structure of streamline downstream of $-\pi/2$, the point at which this streamline is tangent to the boundary.

Now:

$$\zeta(-\pi/2, \varepsilon/2, t) = \sin(k(-3\pi/2 + \varepsilon^{1/2}) + \omega(t - \pi + \varepsilon^{1/2}) + O(\varepsilon))$$

and:

$$\begin{aligned}\zeta(-\pi/2, \varepsilon/2, t) - \zeta(-\pi/2, 0, t) &= \sin(k(-3\pi/2 + \varepsilon^{1/2}) + \omega(t - \pi + \varepsilon^{1/2}) + O(\varepsilon)) \\ &\quad - \sin(k(-\pi/2) + \omega t) \\ &= \sin(k(-\pi/2) + \omega t)[\cos((k + \omega)(\pi - \varepsilon^{1/2}) \\ &\quad + O(\varepsilon)) - 1] - \cos(k(-\pi/2) \\ &\quad + \omega t)\sin((k + \omega)(\pi - \varepsilon^{1/2}) + O(\varepsilon)) \\ &= O(1) \quad \text{as } \varepsilon \to 0,\end{aligned}$$

unless $(k + \omega) = 0$, so the solution fails to be differentiable at the lower boundary. This simple characterization of the condition for smooth solutions should be recognized as a global condition. In general, there need be no systematic relation at all between remote boundary values such as those specified at the top and bottom in this special example. Fig. 2 shows a map of this solution with $B(x, t) = \sin(x + 1.2t)$. Sharp cross stream gradients appear as wavelike patterns in ζ downstream of the point $(-\pi/2, 0)$ as a consequence of the jump in ζ across that characteristic at that point. The process of kinematic frontogenesis may be described in a similar manner. Such a description appears in Staniforth et al. (1987) and Smolarkiewicz (1987) in which an exact solution of an equation describing advection of a passive scalar by a deformation flow is presented. Their exact solution has the property that an observer sitting on certain fluid parcels would observe nearby parcels to be swiftly replaced by parcels carrying different values of the advected scalar which originate at remote locations (see the discussion on page 898 of Staniforth et al.). Thus the formation of the singularity illustrated at the bottom of Fig. 2 is kinematically similar to the formation of sharp gradients in deformation flow, but the singularity we describe in the present work arises as a consequence of incompatible specification of boundary conditions, and will occur even in cases in which the flow in whose domain the open region is embedded is very smooth.

An analysis similar to that given in the preceding paragraphs shows unbounded vorticity gradients in neighborhoods of points such as $(-\pi/2, 2)$ and $(\pi/2, 0)$ where $\zeta(\pi/2, \varepsilon, t) = O((k + \omega)\varepsilon^{1/2})$. This is similar to the singularities found in the solution found earlier of eq. (6). One such singularity appears in Fig. 2 near the point $(-\pi/2, 2)$. Characteristics passing near that point do not originate at remote points, and do not carry discontinuities in ζ itself into the interior. As noted in the previous section, Sensenig's existence and smoothness proof avoids all of these problems. Singularities like the one at $(-\pi/2, 2)$ are avoided by requiring the initial and boundary conditions to be constant in a neighborhood of the characteristic points (see Fig. 1). Singularities like the one at $(-\pi/2, 0)$ are avoided by restrict-

Table 1. *Summary of numerical experiments*

Run #	Type	Intervals/side	Description
1	2 wave	32	coarse mesh finite difference
2		64	fine mesh finite difference
3		64	finite element
4	perturbed Rossby wave	32	full strength perturbation, coarse mesh
5		64	full strength perturbation, intermediate mesh
6		128	full strength perturbation, fine mesh
7		32	half strength perturbation, coarse mesh
8		64	half strength perturbation, intermediate mesh
9		128	half strength perturbation, fine mesh
10		32	half strength perturbation, filtered

ing the time domain of the smooth solution. Solutions to the initial/boundary value problem for eq. (7) could similarly be shown to be smooth for short time by requiring the initial values of ζ to be constant for $-\pi/2-\sigma<x<-\pi/2+\sigma$, $0<y<\sigma$ and restricting the time to be less than σ. Since the maximum advection speed is unity in both the x and y directions, there will not be sufficient time for the characteristics to carry the news of the incompatible vorticity specified upstream.

4. Computational examples

Evidence of the phenomena described in the previous section was sought by application of two models. The first was the finite element Harvard open ocean model (Miller et al., 1983). The second was a finite difference model of the Arakawa type. Both solve the barotropic potential vorticity equation, with initial and boundary conditions chosen to highlight the behavior in question. In this series of runs we wished to investigate the questions of whether practical numerical models exhibit large vorticity gradients near tangent points, and whether these large vorticity gradients can appear in the interior of the region. We exhibit two cases of calculations with perturbed Rossby waves, in which distinctive patterns resembling the analytical example shown in Fig. 2 appears. Effects of filtering are considered, and an example is presented.

We used the two models to solve the barotropic quasigeostrophic equations of conservation of potential vorticity on the β-plane which we write in the form:

$$\zeta_t + J(\psi,\zeta) + \psi_x = 0, \tag{9a}$$

$$\nabla^2\psi = \zeta. \tag{9b}$$

Details of the finite element implementation of the CFvN boundary conditions are given in Miller et al. (1983). The finite difference scheme includes a nine point Arakawa Jacobian in the interior, a six point Jacobian at the edges and a four point Jacobian at the corners. A five point Laplacian was used with an exact direct Poisson solver to calculate the streamfunction diagnostically from the vorticity. The CFvN boundary conditions were implemented by computing the vorticity on the entire boundary and then overwriting the computed boundary vorticity with data at inflow points. The domain was a square centered at the origin. A summary of the computations performed for this section is shown in Table 1.

In our first series of experiments, initial and boundary conditions are given as follows:

$$\psi = \sin(x + y + \tfrac{1}{2}t) + \sin(x + t),$$

$$\zeta = \nabla^2\psi.$$

It is easily verified that even though each of the two waves is a solution to (9), their sum is not, and no first order cross-modulation product will produce a resonance. Furthermore, it can be shown that the initial and boundary conditions are not smoothly compatible, since:

$$\left[\frac{\partial}{\partial t}\zeta_{\text{inflow}}\right|_{\text{initial}} + [\{J(\psi,\zeta)+\psi_x\}_{\text{initial}}]_{\text{inflow}} \neq 0. \tag{10}$$

The basin was chosen to be a square 8 (dimensionless) units on a side. Spatial scales for models such as these are typically chosen to be the local value of the first internal radius of deformation; a representative value for the North Atlantic would be 50 km, so our model basin represents a region of the order of hundreds of km wide. The finite difference code was run with two uniform meshes with 32 and 64 intervals on each side; the finite element code was run only with the finer resolution. The time step was chosen to be 0.025 in the coarse mesh run and half that in the fine mesh runs. The finite element case is considered a fine mesh run. These time steps are rather conservative, since we expect phase and advection speeds of order unity and the mesh width is 0.25 in the coarse resolution case. The results of these tests are shown in Figs. 3 and 4. Normal derivatives of the vorticity fields were computed at selected characteristic points. The selected points are marked on Fig. 4 and the results summarized in Table 2.

Fig. 3 shows the evolution of the streamfunction field in runs 1, 2 and 3. These fields are seen to be quite similar; little is apparently gained from the increased resolution, and the finite difference and finite element solutions also appear quite similar. The vorticity fields shown in Fig. 4 tell a different story. At $t = 2.4$, 96 steps into the coarse mesh run and 192 steps into the other two runs, differences are discernible between the finite difference and the finite element runs, but the two finite difference runs are quite similar. The finite element simulation is distinctly rougher, showing disturbances with two gridpoint wavelength in the east and southwest. The normal derivatives at the westernmost of the two turning points on the southern boundary (note marked points) appear to double approximately as the mesh width is halved, as we might expect from our analysis. This is indicative of a *discontinuity* in the vorticity field. The analogous normal derivative in the finite element case lies between the values of the two finite difference cases.

Further along in time, at $t = 4.8$, the three runs are quite different. In the two finite difference runs, the jagged wavelike patterns in the southwest quadrant roughly double in wavenumber between the coarse and fine mesh runs, and the vorticity gradient at the southern edge of the

Table 2. *Values of normal derivatives of vorticity at selected points* (see Fig. 4)

run description	$T = 2.4$	$T = 4.8$
FD coarse	6.25	-13.4
FD fine	11.77	-16.8
FE	-8.00	-14.24

feature in the northwest roughly doubles. The finite element simulation shows the same features but is rougher than the finite difference simulations, showing strong interior gradients and concentrations of vorticity that do not appear in the other two. The normal derivatives at marked points no longer double as the mesh width is halved.

In our first series of experiments, the initial and boundary conditions were not smoothly compatible with the model (see eq. (10)). In our next series of experiments, runs 4–10, the initial and boundary values chosen were derived from a perturbed Rossby wave. The particular perturbation used was chosen so that the initial and boundary conditions would be compatible, unlike the previous series. The streamfunction was the sum of the Rossby wave and a bilinear function of x and y which was modulated sinusoidally at the frequency of the Rossby wave. Since the perturbation was bilinear, the initial vorticity and the vorticity at inflow were unaffected. The initial and boundary conditions were given by:

$$\psi = \sin(\kappa x + \lambda y + \omega t) + \mu \sin(\omega t) \times \left[\frac{X - 2x}{2X}\right]\left[\frac{Y - 2y}{2Y}\right]$$

where:

κ = the zonal wavenumber = 1
λ = the meridional wavenumber = 1
$\omega = \kappa/(\kappa^2 + \lambda^2)$ = the Rossby wave frequency
X = the zonal basin extent = 8 (dimensionless)
Y = the meridional basin extent = 8 (dimensionless)
μ = the perturbation strength
= X in runs 1–3
= $X/2$ in runs 4–7.

Clearly the initial and boundary conditions yield the same value for on the boundary at time

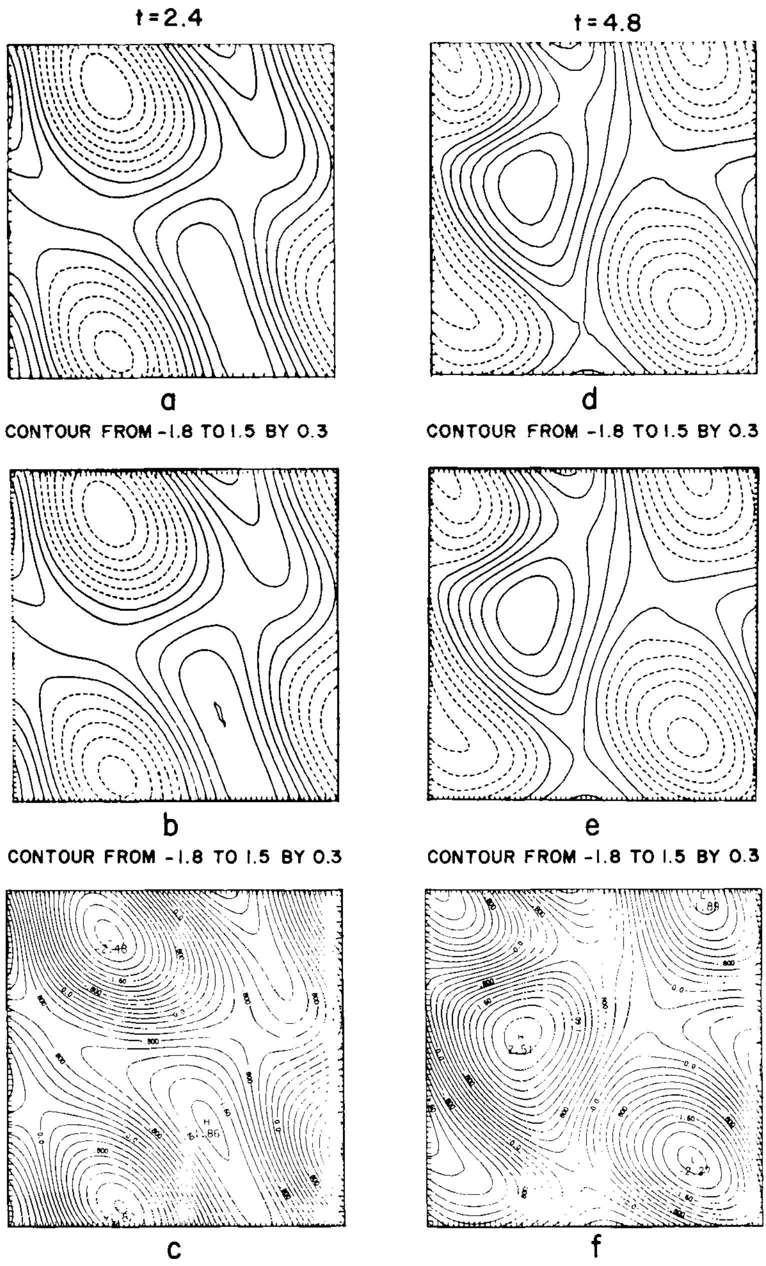

Fig. 3. Evolution of streamfunction fields for the coarse and fine finite difference runs and the finite element run (experiments 1–3; see Table 1). Left column (a, b, c) represents $t = 2.4$, 96 steps in the coarse resolution run, 192 steps in the others. Right hand column are the fields at $t = 4.8$. (a, d) Coarse resolution finite difference run. (b, e) Fine resolution finite difference run. (c, f) Finite element run. Tick marks represent grid spacing.

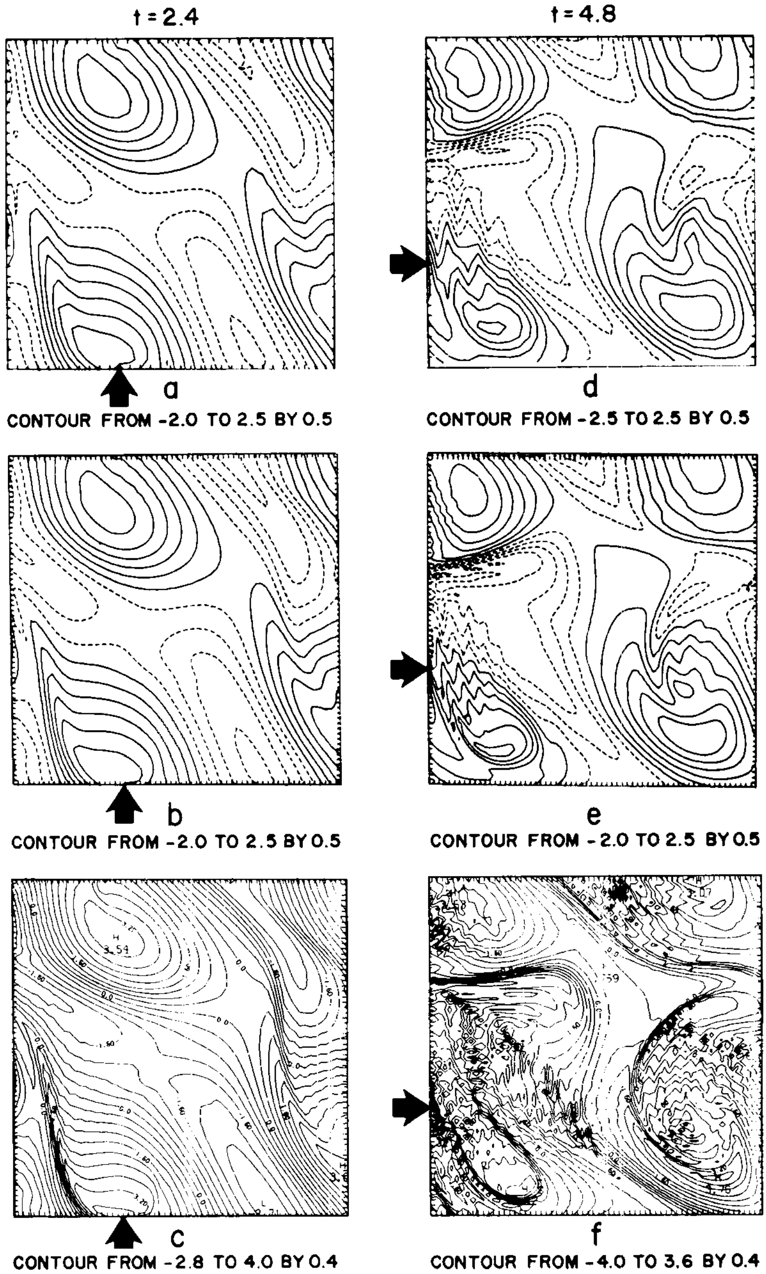

Fig. 4. Evolution of vorticity fields for the coarse and fine finite difference runs, and the finite element run. Left column (a, b, c) represents $t = 2.4$, 96 steps in the coarse resolution run, 192 in the others. Right column (d, e, f) represents $t = 4.8$. (a, d) Coarse resolution finite difference. (b, e) Fine resolution finite difference run. (c, f) Finite element run. Arrows on boundaries represent points at which normal derivatives are calculated; see Table 2.

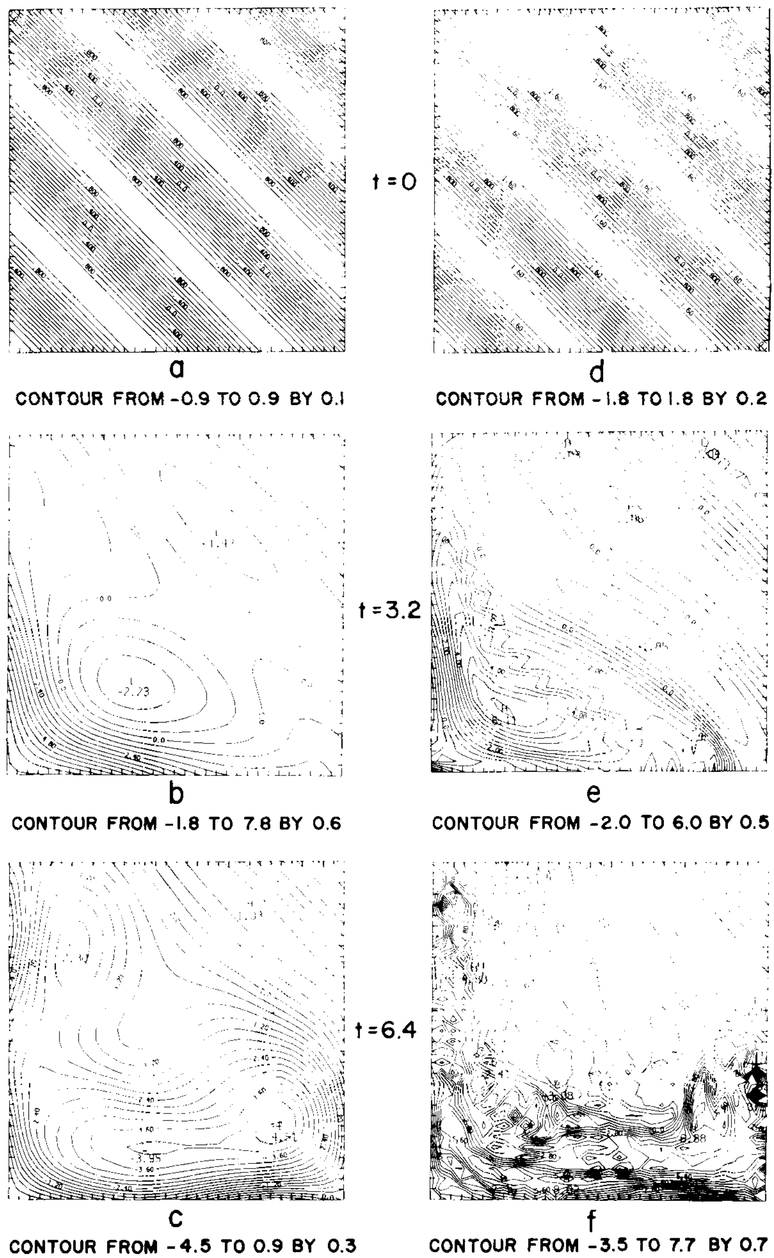

Fig. 5. Evolution of the simulation with the boundary and initial conditions taken to be the sum of a Rossby wave and a perturbation which is bilinear in space and sinusoidal in time, with period 4π, the same as the underlying Rossby wave. Results from run number 4 (see Table 1), the coarsest resolution run, 32 intervals in the basin width. Tick marks indicate grid spacing. Left column (a, b, c) and (g, h, i) depicts the evolution of the streamfunction field, beginning at $t = 0$, in (scaled) time steps of 3.2. Right column (d, e, f) and (j, k, l) depicts the corresponding vorticity fields.

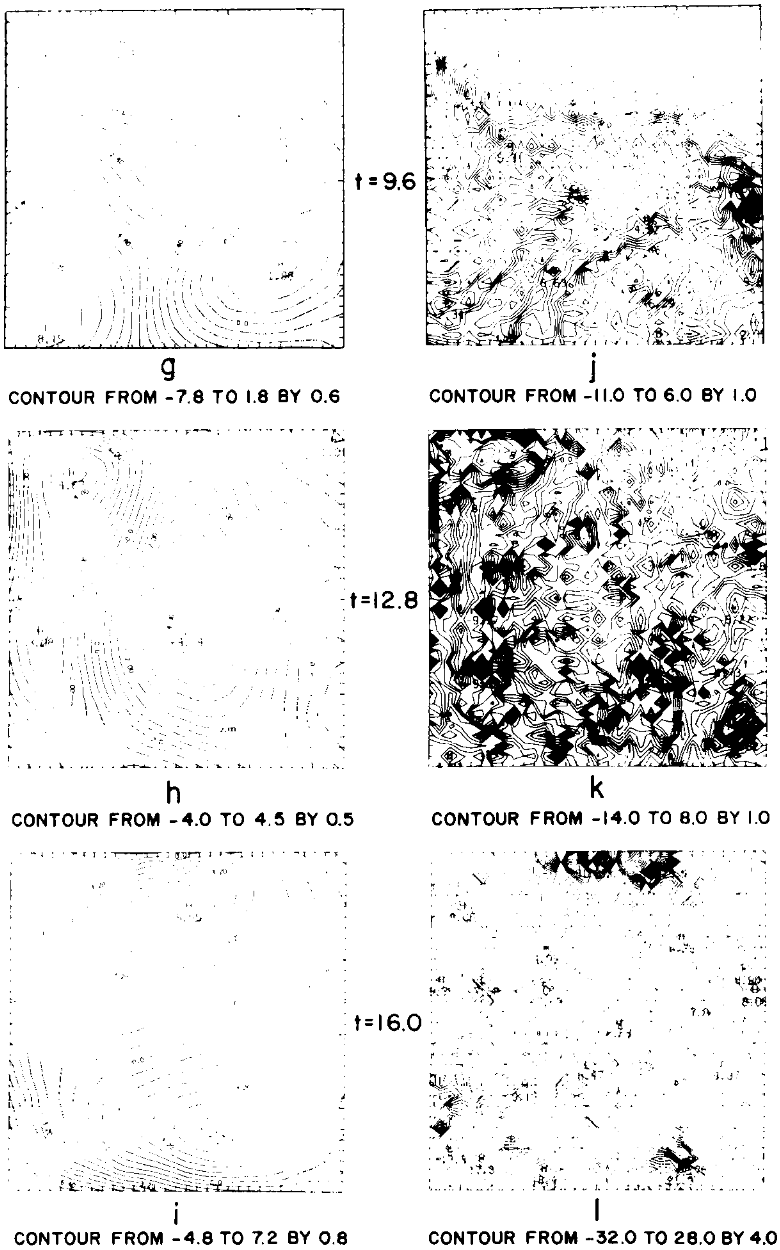

Fig. 5 (continued).

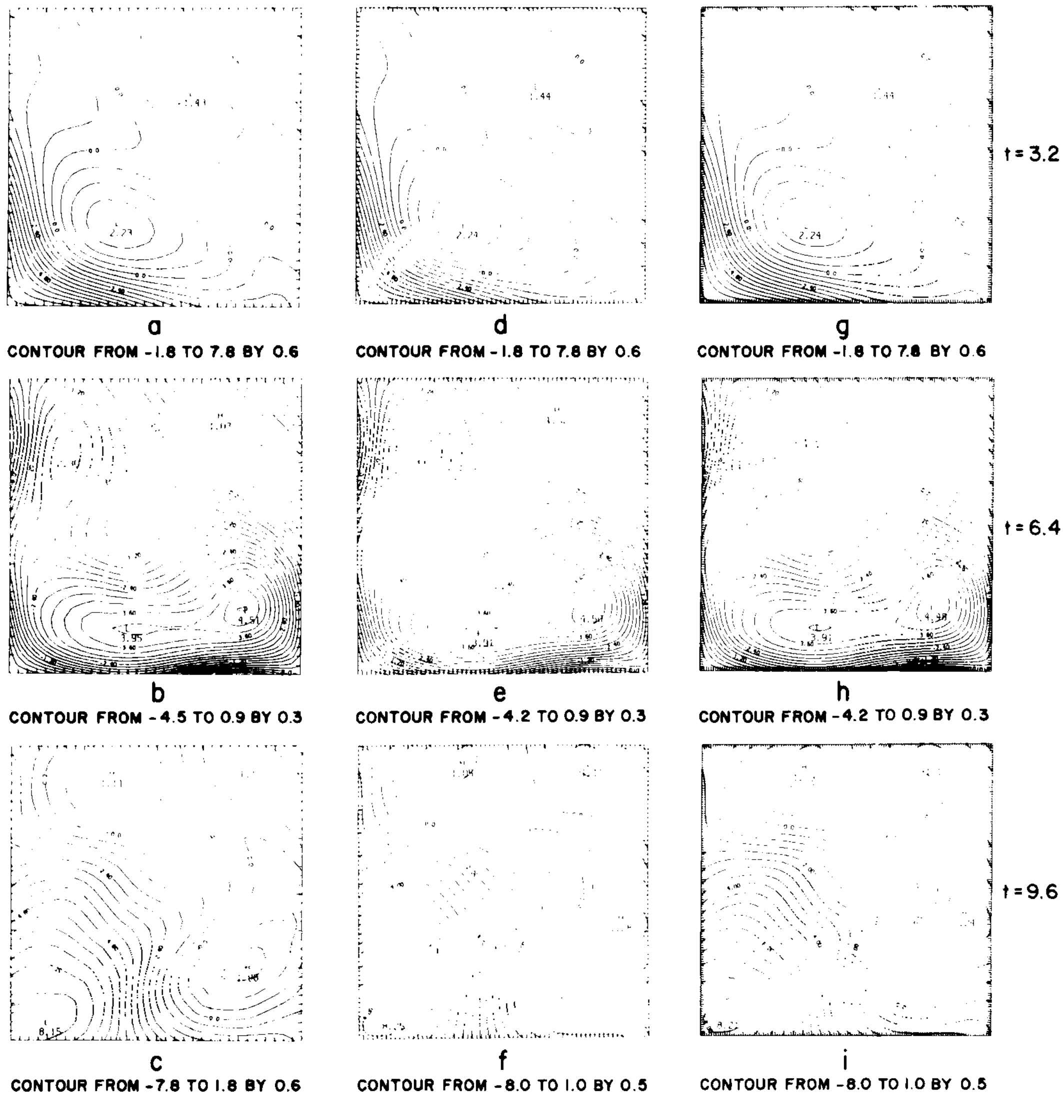

Fig. 6. Evolution of the streamfunction in three perturbed Rossby wave runs with successively refined resolution. (a, b, c) Streamfunction fields at times 3.2, 6.4 and 9.6, respectively; identical to Fig. 5b, c, d. (d, e, f) as (a, b, c), but with twice the resolution (run number 5; see Table 1). Time step is halved from run number 4 (a, b, c) to preserve stability characteristics. (g, h, i) As (d, e, f), but with twice the resolution, i.e., 4 times the resolution of (a, b, c) (run number 6). Time step again halved. Tick marks in all frames represent grid spacing.

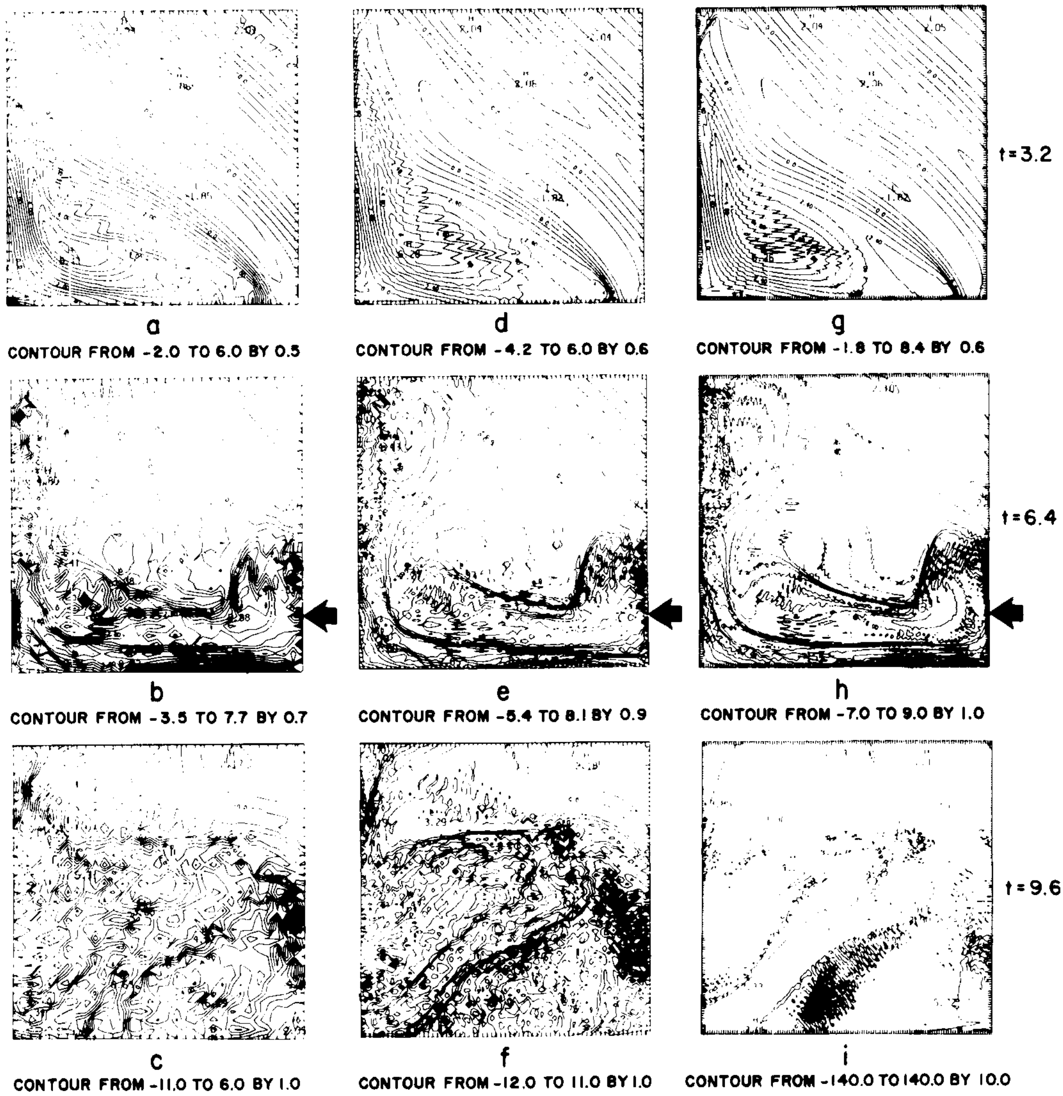

Fig. 7. Evolution of the vorticity in three perturbed Rossby wave runs with successively refined resolution. (a, b, c) Vorticity fields at times 3.2, 6.4 and 9.6, respectively; identical to Fig. 5h, i, j. (d, e, f) As (a, b, c), but with twice the resolution (run number 5). Time step is halved from run number 4 to preserve stability characteristics. (g, h, i) As (d, e, f), but with twice the resolution, i.e., 4 times the resolution of (a, b, c). Tick marks in all frames represent grid spacing. The arrow marks the origin for Fig. 8.

zero, and the initial and boundary vorticities agree on the initial inflow set. It can also be shown that, in contrast with (10):

$$\left[\frac{\partial}{\partial t}\zeta_{\text{inflow}}\right]_{\text{initial}} + [\{J(\psi,\zeta)+\psi_x\}_{\text{initial}}]_{\text{inflow}} = 0,$$

but:

$$\left[\frac{\partial^2}{\partial t^2}\zeta_{\text{inflow}}\right]_{\text{initial}} + \left[\frac{\partial}{\partial t}\{J(\psi,\zeta)+\psi_x\}_{\text{initial}}\right]_{\text{inflow}} \neq 0.$$

The model was run with three uniform grids: 33×33, 65×65 and 129×129, including boundary points. The 33×33 case was run with time steps of 0.003125, and the time steps were refined in proportion to the grid size for the finer spatial resolution runs.

Fig. 5 shows the evolution of the streamfunction and vorticity fields for run #4, the coarse spatial resolution case. The period of the forcing functions at the boundary was 4π, so even in this case of coarsest time resolution there are more than 2000 steps per period. This is much finer temporal resolution than had been used in previous studies with the Harvard model.

As early as $t = 3.2$, just over one quarter period into the simulation, large vorticity gradients can be observed in the interior in the southwest quadrant, running roughly northwest to southeast. At $t = 6.4$, large vorticity gradients appear along the southern, eastern and western boundaries, and small scale structure dominates the southern half. Along the southern and eastern boundaries, these regions of strong vorticity gradient appear to be associated with flow tangent to the boundary. At $t = 12.8$, just over a period into the simulation, the vorticity is concentrated in small areas in the interior, and there is little apparent large scale structure. A new band of large gradient is seen forming on the western boundary, near the northernmost of the two tangent points on that boundary. By $t = 16$, the vorticity field is dominated by concentrated features on the northern boundary. The roughness of the vorticity field is now apparent in the streamfunction field near the northern boundary. Note also that the vorticity has grown. Initially it ranged from -2 to 2; by this time, it ranges from -32 to 28. The conservative numerical scheme used here preserves total kinetic energy, vorticity and enstrophy, but can not guarantee that the vorticity of each fluid parcel will remain constant. Since the perturbation to the initial Rossby wave contributes no vorticity, there should be no point in the fluid where the vorticity is outside of its initial range. Vorticity values as great as the extremes observed here indicate a rather serious failure of the model to estimate vorticity.

Experiments 5 and 6 were conducted with identical initial and boundary conditions to experiment 4, but with refined grids. Experiment 5 was performed with twice the resolution of experiment 4 and experiment 6 was performed with four times the resolution, i.e., 128 intervals on each side of the square model region. The results are shown in Figs. 6 and 7. Results of experiment 4 are also shown for comparison. Fig. 6 shows the evolution of the streamfunction fields in runs 4, 5 and 6. These fields are quite similar; note, for example, the field at $t = 9.6$ for the intermediate and highest resolution cases. These fields are essentially identical within graphical accuracy. The same can not be said of the vorticity fields shown in Fig. 7. At $t = 3.2$ and $t = 6.4$, the maps have much in common qualitatively, but the gradients do not appear to converge. At $t = 3.2$, the wave structures just southwest of the center which run roughly northwest to southeast double in wavenumber with doubled resolution. At $t = 6.4$, thin bands of strong vorticity gradients dominate the southern halves of the fields, and the vorticity gradients here, too, appear to double with doubled resolution. By $t = 9.6$, the fields are dominated by small scale features, and the resemblance between them is not nearly so apparent.

While the slope of the vorticity at the boundary in these simulations does not converge in any obvious way, the nature of actual divergence is not immediately clear from these experiments. Fig. 8 shows vorticity plotted in the direction normal to the boundary in the vicinity of a point where the flow is tangent to the region for runs 4, 5 and 6. The point chosen is on the eastern boundary at southernmost of the two tangent points. The point is marked on Fig. 7. The slope of the vorticity clearly increases with increasing resolution, more than doubling from run 4 to run 5, and not quite doubling from run 5 to run 6.

In the next series of experiments, runs 7, 8 and 9, the strength of the perturbation to the Rossby wave was halved. From the theory and from our analytical examples, we expect these same large

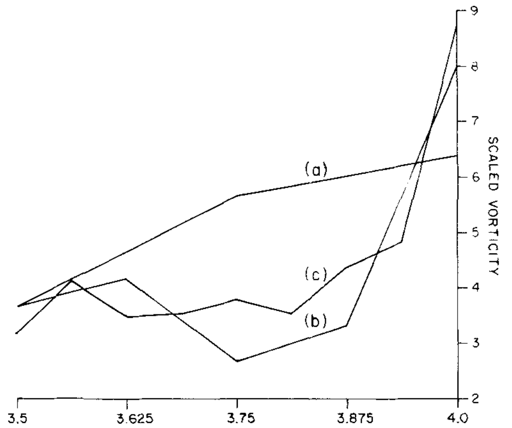

Fig. 8. Vorticity versus x, plotted inward from a selected point on the eastern boundary at $t = 6.4$ in runs 4–6; see Fig. 7 for location of the point. The basin is 8 units wide, with the origin at the center. Both x and the vorticity are dimensionless. The streamline running through this point is tangent to the boundary. (a, b, c) Depicts runs 4, 5 and 6, the coarse, intermediate and finest mesh, respectively.

(theoretically unbounded) vorticity gradients to appear, even with the weaker perturbation.

Fig. 9 shows the evolution of the computed fields for the coarse resolution half strength perturbation case. By $t = 3.2$, the vorticity field is dominated by small scale structure in the southern half of the region, with structure resembling the full strength perturbation case. By $t = 12.8$, little large scale structure remains in the vorticity field at all, and the streamfunction field shows considerable roughness. A plot of vorticity in the direction normal to the boundary at the southern tangent point on the eastern edge appears in Fig. 10. In this case, we do observe doubling of the slope of the vorticity with doubling of the resolution. This is the effect expected from theoretical considerations. The gradient of the vorticity is expected to be unbounded near points where the flow is tangent to the domain. One therefore expects the normal derivatives of the vorticity to diverge. Furthermore, because the classical theory prescribes a compatibility condition which is not met by our perturbed Rossby wave simulations, this divergence is expected to persist even when the perturbation is weakened.

One obvious practical consideration is the effect of filtering upon the numerical results presented above. Clearly, filtering the vorticity field will eliminate the gridscale features which come to dominate the fields in the examples shown above. In order to get a general idea of the effect of filtering in the cases shown here, we ran an experiment with a fourth order Shapiro filter (see Miller et al., 1983 for details) applied to the vorticity field at each time step. Fig. 11 shows the results of that run. It is interesting to compare Fig. 11 with Fig. 9, which differs only in the fact that run number 7, from which Fig. 9 was taken, was unfiltered. At $t = 3.2$, both the streamfunction and vorticity fields are similar. As expected, the filter has smoothed out the wiggles in the vorticity maximum in the southwest. At $t = 6.4$, the streamfunction fields are very much alike, especially in the northern half of the field, as expected. The vorticity fields are also somewhat alike. The Rossby wave structure in the northeast is preserved, as is the cyclonic feature in the northwest. The southern half, which is dominated by small scale structure in the unfiltered run, appears smooth in the filtered run, and it is possible to see a resemblance. But by $t = 9.6$, both the streamfunction fields and the vorticity fields are very different in the filtered and unfiltered cases. A maximum in the vorticity field appears in the filtered case near the western edge which has no counterpart in the unfiltered run. More interestingly, the streamfunctions fields are qualitatively different. The large cyclone in the lower half of the unfiltered field and the weaker anticyclone in the northern part of that field have disappeared, to be replaced by a large anticyclone roughly in the center. The Rossby wave structure in the northeast corner remains. In this run, the filter did smooth out the vorticity field, but by $t = 9.6$, roughly three quarters of a period, the streamfunction fields were qualitatively different from the unfiltered cases.

5. Summary and conclusions

It is known from the classical theory of boundary value problems that prescription of data on a characteristic surface gives rise to compatibility conditions which must be met in order to formulate a consistent boundary value problem. The theory is very well developed for hyperbolic

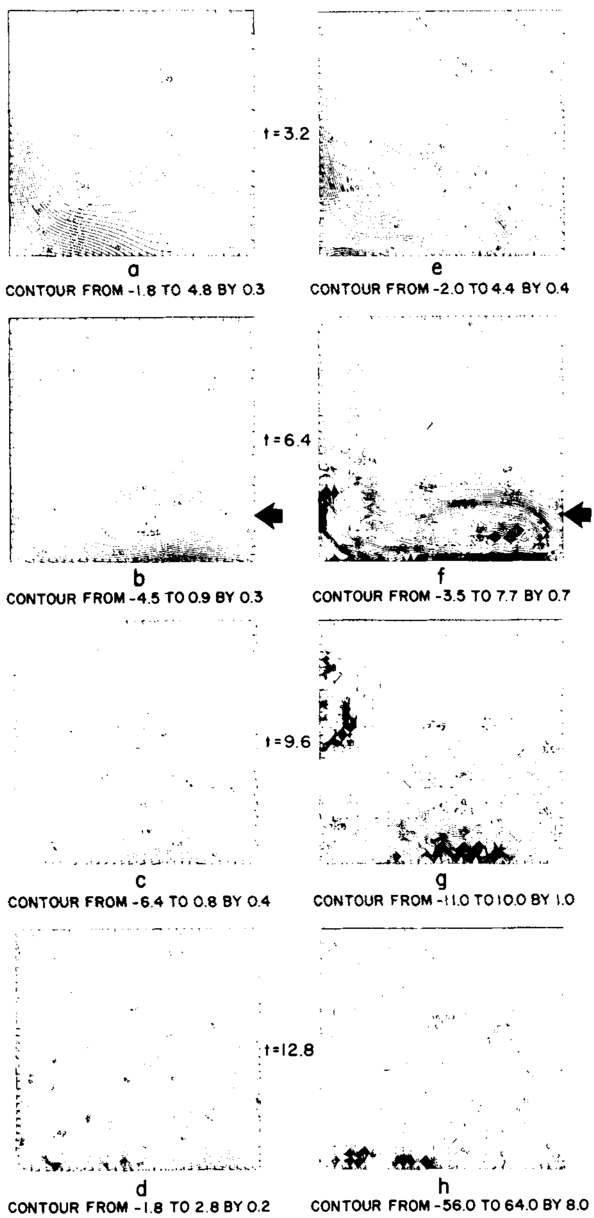

Fig. 9. Evolution of the streamfunction using the perturbed Rossby wave with perturbation half the strength of previous cases (experiment 7). This is the coarse resolution run with 32 intervals in the basin width. (a, b, c, d) Streamfunction fields at $t = 3.2$, 6.4, 9.6, 12.8. (e, f, g, h) Vorticity fields corresponding to (a, b, c, d). The arrow marks the origin for Fig. 10.

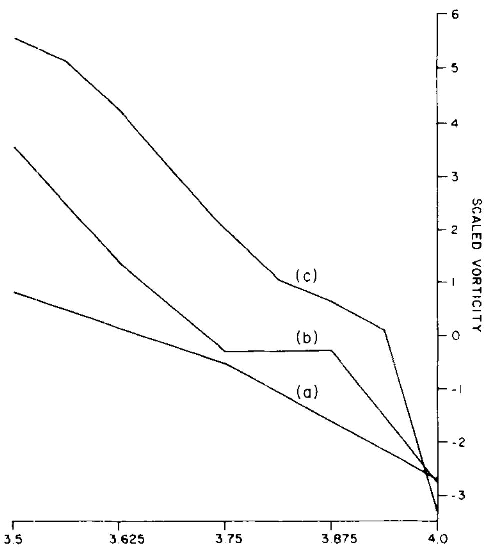

Fig. 10. Vorticity versus x, plotted inward from a selected point on the eastern boundary at $t = 6.4$ in runs 7–9 (half strength perturbation). See Fig. 9 for location of this point. Both x and the vorticity are dimensionless. The basin is 8 units wide, centered at the origin.

equations, but it is not so well developed for the quasigeostrophic model, which has only one family of characteristics. The most common boundary conditions used in open boundary quasigeostrophic simulations are those first proposed in CFvN, but the example given in CFvN to motivate that choice of boundary conditions was a case of a non-simply connected domain, in which the characteristics were nowhere tangent to the boundary. This problem can not be so easily avoided in open ocean simulations. A survey of the partial differential equations literature shows that weak solutions of the problem exist under rather general circumstances, but do not, in general, have bounded vorticity gradients. This is not surprising, but it is a potential problem for practical numerical codes, most of which (explicitly or implicitly) differentiate the vorticity. One might expect that finite element methods might not suffer because of their relation with the weak formulation of the equations, but the expected large gradients do in fact appear in finite element simulations.

In order to shed some light on the problem, very simple analytical examples were derived which exhibit the extreme behavior we seek. In these examples, simplified models were derived which possess solutions with some of the properties sought.

A variety of numerical experiments was then performed, beginning with an example which violated the simplest compatibility condition. Finite difference and finite element methods were used to calculate solutions, and the results were consistent with the hypothesis that the normal derivative of the vorticity diverges with increasing resolution near points where the flow is tangent to the boundary.

In the second series of experiments, initial and boundary conditions were sampled from a perturbed Rossby wave which was carefully chosen to be smoothly compatible with the equation. Mesh refinement experiments were performed with the finite element model, and the normal derivative of the vorticity was again observed to diverge. Further experiments with weaker perturbations showed similar behavior.

One obvious practical solution to the problem is the addition of artificial dissipation, or filtering. One filtered experiment was performed, and, while the resulting vorticity field was quite smooth, the streamfunction fields were qualitatively different from those in the unfiltered case, and the streamfunction in the unfiltered cases had converged nicely with increasing resolution. Filtering must clearly be applied with caution.

To some readers, it may appear at first glance that our examples are artificial ones, to the extent of having questionable relevance to practical ocean forecasting. The most obvious point to consider is that these are permissible inputs to the models, and, to our knowledge, no screening procedure has been suggested to protect models from this sort of trouble. There is, however, a more important point to consider. The fact is that our examples are artificially well behaved. The perturbed Rossby wave example was specifically designed to be smoothly compatible with the model. Operational models will not be so lucky.

The clearest practical implication of these results is that incompatible boundary conditions are unavoidable in practice, and the boundary instability documented here will cause practical models to fail on time scales comparable to those which characterize the boundary conditions. This

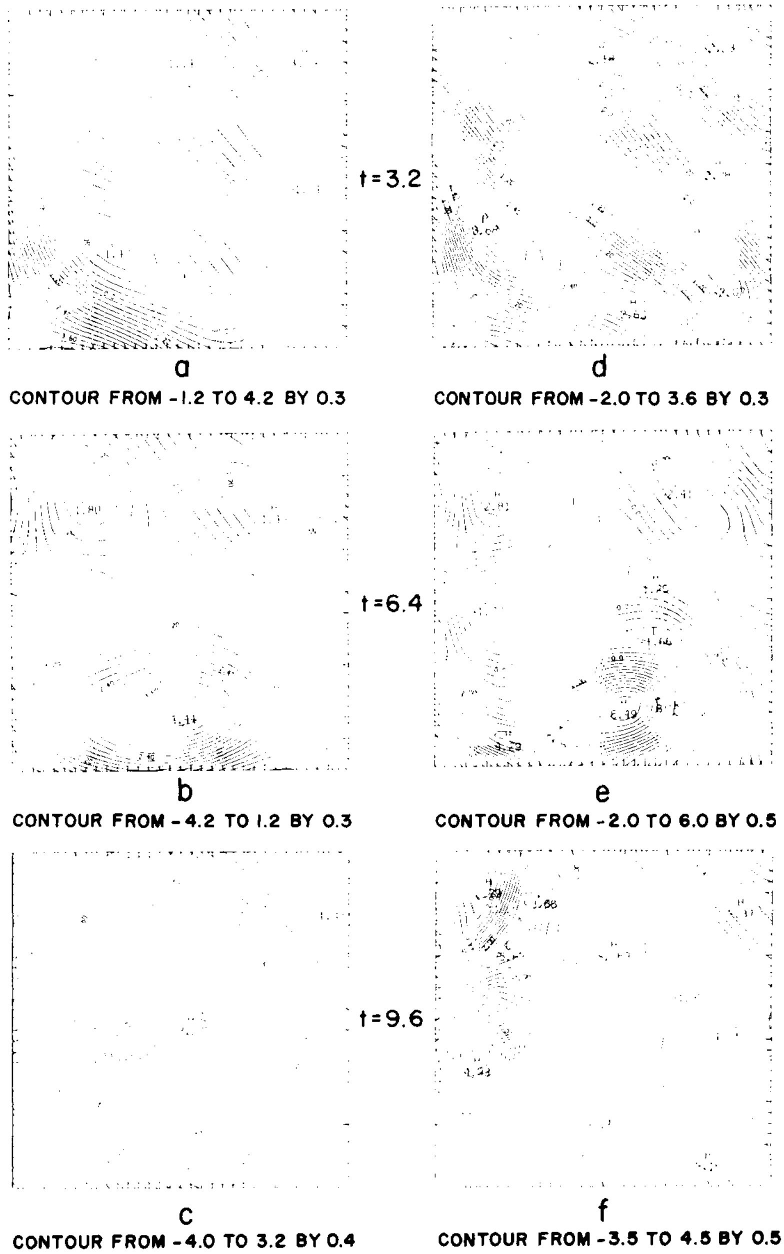

Fig. 11. Evolution of streamfunction and vorticity in filtered run (experiment 10); as 9 but filtered. (a, b, c) Streamfunction fields at $t = 3.2$, 6.4, 9.6. (d, e, f) Vorticity fields corresponding to (a, b, c).

highlights the role of data assimilation in practical open ocean forecasting. New data must be introduced in the interior at intervals which are short compared to forcing time scales.

6. Acknowledgements

This work was supported by Office of Naval Research contract N00014-84-C0132, and by the Institute for Naval Oceanography, where R.N.M. was a visitor during the summer of 1986. Some of the computations were performed at the Central Computer Facility of the Naval Research Laboratory, Washington, D.C., with ONR support. We thank the staff of that facility for their help. Some of the computations were performed at NCAR, which is supported by the National Science Foundation. We would like to thank J.-Y. Sun of Shandong University and Eugene Isaacson of the Courant Institute of Mathematical Sciences for helpful discussions, and Michael Ghil of UCLA for his help in obtaining the Sensenig manuscript. A.F.B. acknowledges the assistance of Sean O'Connor with computations.

REFERENCES

Bardos, C., Leroux, A. Y. and Nedelec, J. C. 1979. First order quasilinear equations with boundary conditions. *Comm. in PDE 4*, 1017–1034.

Bennett, A. F. and Kloeden, P. E. 1978. Boundary conditions for limited area forecasts. *J. Atmos. Sci. 35*, 990–996.

Charney, J. G., Fjørtoft, R. and von Neumann, J. 1950. Numerical integration of the barotropic vorticity equation. *Tellus 2*, 237–254.

Fix, G. J. 1975. Finite element models for ocean circulation problems. *SIAM J. Applied Math. 29*, 371–387.

Forsythe, G. and Wasow, W. 1960. *Finite difference methods for partial differential equations*. New York: J. Wiley and Sons, Inc., 444 pp.

Judovich, V. I. 1964. Two-dimensional non-stationary problem of the flow of an ideal incompressible fluid through a given region. *Mat. Sb. (new series) 64*, 562–588.

Kochin, N. F. 1980. On an existence theorem in hydrodynamics. Transl. by T. P. Baranowski and P. E. Kloeden. *GFDL Report No. 66*, Geophysical Fluid Dynamics Laboratory, Monash University, Victoria, Australia, 37 pp.

Majda, A. and Osher, S. 1975. Initial-boundary value problems for hyperbolic equations with uniformly characteristic boundary. *Comm. Pure Appl. Math. 28*, 607–675.

Miller, R. N. and Robinson, A. R. 1984. Dynamical forecast experiments with a baroclinic quasigeostrophic model. In *Predictability of fluid motions* (eds. G. Holloway and B. J. West). New York: American Institute of Physics, 457–472.

Miller, R. N., Robinson, A. R. and Haidvogel, D. B. 1983. A baroclinic quasigeostrophic open ocean model. *J. Comput. Phys. 50*, 38–70.

Robinson, A. R. and Leslie, W. G. 1985. Estimation and prediction of oceanic eddy fields. *Prog. Oceanogr. 14*, 485–510.

Robinson, A. R., Carton, J. A., Mooers, C. N. K., Walstad, L. J., Carter, E. F., Rienecker, M. M., Smith, J. A. and Leslie, W. G. 1984. A real-time dynamical forecast of ocean synoptic mesoscale eddies. *Nature 309*, 781–783.

Sensenig, C. B. 1959. *Existence and uniqueness for a third order non-linear partial differential equation*. New York University Institute of Mathematial Sciences IMM-NYU 258, 60 pp.

Smolarkiewicz, P. K. 1987. Reply. *Mon. Wea. Rev. 115*, 901–902.

Staniforth, A., Cote, J. and Pudykiewicz, J. 1987. Comments on "Smolarkewicz's deformational flow." *Mon. Wea. Rev. 115*, 894–900.

Sundström, A. 1969. Stability theorems for the barotropic vorticity equation. *Mon. Wea. Rev. 97*, 340–345.

Whitham, G. B. 1974. *Linear and Nonlinear Waves*. New York: J. Wiley and Sons, Inc., 636 pp.